Extending the Spectrum of *EYS*-Associated Retinal Disease to Macular Dystrophy

Laurence H. M. Pierrache,[1–4] Muriël Messchaert,[5,6] Alberta A. H. J. Thiadens,[3] Lonneke Haer-Wigman,[5] Yvonne de Jong-Hesse,[7] Wendy A. G. van Zelst-Stams,[5] Rob W. J. Collin,[5,6] Caroline C. W. Klaver,[3,4,8] and L. Ingeborgh van den Born[1,2]

[1]The Rotterdam Eye Hospital, Rotterdam, The Netherlands
[2]Rotterdam Ophthalmic Institute, Rotterdam, The Netherlands
[3]Department of Ophthalmology, Erasmus Medical Center, Rotterdam, The Netherlands
[4]Department of Epidemiology, Erasmus Medical Center, Rotterdam, The Netherlands
[5]Department of Human Genetics, Radboud University Medical Center, Nijmegen, The Netherlands
[6]Donders Institute for Brain, Cognition and Behaviour, Radboud University Medical Center, Nijmegen, The Netherlands
[7]Department of Ophthalmology, Amsterdam UMC, Vrije Universiteit Amsterdam, Amsterdam, The Netherlands
[8]Department of Ophthalmology, Radboud University Medical Center, Nijmegen, The Netherlands

Correspondence: L. Ingeborgh van den Born, the Rotterdam Eye Hospital, Schiedamse Vest 180, 3011 BH Rotterdam, The Netherlands; born@eyehospital.nl.

Submitted: August 17, 2018
Accepted: March 27, 2019

Citation: Pierrache LHM, Messchaert M, Thiadens AAHJ, et al. Extending the spectrum of *EYS*-associated retinal disease to macular dystrophy. *Invest Ophthalmol Vis Sci*. 2019;60:2049–2063. https://doi.org/10.1167/iovs.18-25531

Purpose. To assess the phenotypic variability and natural course of inherited retinal diseases (IRDs) caused by *EYS* mutations.

Methods. Multiethnic cohort study ($N = 30$) with biallelic *EYS* variants from a clinical IRD database (retinitis pigmentosa [RP], $N = 27$; cone-rod dystrophy [CRD], $N = 1$; and macular dystrophy, $N = 2$). In vitro minigene splice assay was performed to determine the effect on *EYS* pre-mRNA splicing of the c.1299+5_1299+8del variant in macular dystrophy patients.

Results. We found 27 different *EYS* variants in RP patients and 7 were novel. The rate of visual field loss of the V4e isopter area was -0.84 ± 0.44 ln(deg^2) per year, and the rate of visual acuity loss was 0.75 Early Treatment Diabetic Retinopathy Study letters per year. Ellipsoid zone width was correlated with area of the hyperautofluorescent ring, with $r_s = 0.78$ and $P < 0.001$. Rate of decline in ellipsoid zone width was -57 ± 17 µm per year ($P < 0.01$) ($n = 14$) or $-3.69\% \pm 0.51\%$ from baseline per year ($P < 0.001$). An isolated CRD patient carried a homozygous *EYS* variant (c.9405T>A), previously identified in RP patients. Two siblings with macular dystrophy carried compound heterozygous *EYS* variants: c.1299+5_1299+8del and c.6050G>T. The former was novel and shown to result in skipping of exon 8, and the latter was a known RP variant.

Conclusions. We report on *EYS*-associated macular dystrophy, extending the spectrum of *EYS*-associated IRDs. We observed heterogeneity between RP patients in age of onset and disease progression. Identical *EYS* variants were found in cases with RP, CRD, and macular dystrophy. Screening for *EYS* variants in CRD and macular dystrophy patients might increase the diagnostic yield in previously unsolved cases.

Keywords: retinitis pigmentosa, cone-rod dystrophy, macular dystrophy, inherited retinal disease, *EYS*

Inherited retinal diseases (IRDs) are a heterogeneous group of genetic eye diseases characterized by progressive degeneration of photoreceptor and/or retinal pigment epithelium (RPE) cells, leading to severe visual impairment and blindness. Retinitis pigmentosa (RP), a rod-cone dystrophy, is the most common subtype of IRD with an estimated prevalence of 1 in 4000 individuals.[1] Patients report night blindness and visual field (VF) constriction from early adolescence and gradually decreasing visual acuity later in life. Over 250 genes have been described to be mutated in IRD, of which several can be mutated in different clinical subtypes of IRD.[2]

Eyes shut homolog (*EYS*; OMIM: 612424) was first reported in 2008 by two independent groups,[3,4] and both described this gene as the human ortholog of Drosophila "eyes shut" (eys), also known as Spacemaker (spam). Mutations in *EYS* account for ~5% to 35% of European and Asian autosomal recessive retinitis pigmentosa cases[5–11] but have also been described in three patients with autosomal recessive cone-rod dystrophy (CRD).[4,12,13] *EYS* is located on chromosome 6p12 (*RP25* locus), spans over 2 Mb, and consists of 44 exons that together code for a protein that is predicted to harbor 27 epidermal growth factor (EGF)-like domains and 5 laminin G-like domains. There are at least four isoforms, all of which are expressed in the human retina.[14] The Drosophila ortholog plays an important role in retinal morphogenesis and architecture.[15] In zebrafish, *Eys* is expressed in the outer segments and connecting cilium/transition zone (CC/TZ) of both rod and cone photoreceptors.[16–18] Functional studies in zebrafish suggest *Eys* helps to maintain the stability of the ciliary axoneme in both rods and cones and the integrity of the ciliary pocket in cones.[16–18] *Eys* knockout zebrafish showed a cone-rod pattern of retinal degeneration,[16] and the *Eys* protein

was assumed to be essential for the structural integrity of photoreceptor cells.[18] However, the exact function of the EYS protein and the role of the different isoforms in the human retina still remains unclear.

We have assessed the spectrum of retinal disease and the course of visual function in our multiethnic cohort of 30 patients carrying biallelic *EYS* mutations to improve patient counseling on prognosis and to provide guidance for the timing of therapeutic intervention if available. Twenty-seven patients were diagnosed with RP, one patient was diagnosed with CRD, and two patients with macular dystrophy. To find an explanation for the generalized versus more localized retinal dystrophy among our subjects, we performed functional testing of a novel splice site variant and bioinformatically assessed the nature of other (presumed) pathogenic variants.

Materials and Methods

Study Subjects

We gathered all available DNA testing results from IRD patients from two tertiary care hospitals (The Rotterdam Eye Hospital and Erasmus Medical Center) and selected patients with biallelic *EYS* mutations. In total, we included 30 IRD patients from 25 families. Four patients were previously described by Littink et al.[5] Eighteen patients were isolated cases with a negative family history of inherited retinal dystrophies. Twenty-seven patients were diagnosed with RP, one patient with CRD, and two patients with macular dystrophy based on clinical characteristics, retinal imaging, and visual function testing. The study protocol adhered to the tenets of the Declaration of Helsinki and was approved by the Institutional Review Board and the Ethics Committee of the Erasmus Medical Center (Rotterdam, The Netherlands).

Molecular Diagnosis

The molecular diagnosis of *EYS* variants (NM_001142800.1) was made using Sanger sequencing (9 patients), autosomal recessive RP APEX genotyping array (3 patients), and targeted analysis of 286 IRD-associated genes (Supplemental data) after exome sequencing (18 patients). To determine the effect of the c.1299+5_1299+8del variant on EYS pre-mRNA splicing, an in vitro minigene splice assay was performed. For this, we generated a wild-type minigene and a mutant minigene harboring the c.1299+5_1299+8del variant, which each contain exon 8 and parts of the flanking introns of EYS (Fig. 1A). To investigate if the c.1299+5_1299+8del variant leads to alterations in splicing, HEK293T cells were transfected with the wild type or mutant minigene constructs, followed by RT-PCR analysis. A detailed description of the applied techniques is provided in the Supplementary data.

Clinical Work-Up

Data were collected from our own medical charts, and historic data were retrieved from referring ophthalmologists to maximize the follow-up period. Ophthalmologic examination included best-corrected visual acuity (BCVA), Goldmann kinetic VF testing, full-field electroretinogram (ffERG) according to International Society for Clinical Electrophysiology of Vision standards (Diagnosys, Lowell, MA, USA), multifocal electroretinogram (Diagnosys), dilated fundus examination, color fundus photography (D300 [Nikon, Tokyo, Japan]; TRC-NW65; Topcon, Tokyo, Japan; and Zeiss FF 450 Plus Fundus Camera [Carl Zeiss Meditec, Jena, Germany]), spectral-domain optical coherence tomography (SD-OCT) (Spectralis; Heidelberg Engineering GmbH, Dossenheim, Germany), and 30° field fundus autofluorescence (FAF) (Spectralis). Quantative image analysis was performed with Heidelberg Eye Explorer Software. The area inside the hyperautofluorescent ring was measured from the outer border by using a free-hand drawing tool (Supplementary Fig. S1A). The width of the ellipsoid zone was measured in the horizontal foveal B-scan with a distance measurement tool (Supplementary Fig. S1B). VFs were digitized using a method described by Dagnelie.[19] We measured the retinal area of the V4e target because this target was consistently used in all examinations.

Statistical Analysis

Visual impairment was defined as either low vision (BCVA worse than 0.50 logMAR but equal or better than 1.30 logMAR and/or central VF radius of the V4e target smaller than 20° but equal or larger than 10° in the better eye) or blindness (BCVA worse than 1.30 logMAR and/or central VF radius of the V4e target smaller than 10° in the better eye) in accordance with the World Health Organization criteria. We used the Spearman correlation coefficient to analyze the strength and the direction of the association between variables. For analysis of the VF area, the ellipsoid zone width, and the area of the hyperautofluorescent ring on FAF, we used the mean of the right and the left eye as they were significantly correlated (ellipsoid zone $r_s = 0.95$, $P < 0.001$; and hyperautofluorescent ring $r_s = 0.96$, $P \leq 0.001$). To calculate the annual rate of decline in visual function, we used mixed effects linear regression modeling with visual acuity in logMAR and with log-transformed area of the V4e isopter expressed in degrees squared (deg^2) for VF and corrected for repeated measurements by entering a fixed effect.[20] Patients with a single visit were excluded from longitudinal analysis. We used a Student's *t*-test to compare differences in age of onset, age at diagnosis, and age at last examination between patients with and without constricted VFs at last examination. To calculate the annual rate of decline in ellipsoid zone width, we used mixed effects linear regression modeling and corrected for repeated measurements by entering a fixed effect. Additionally, we calculated the rate of decline of the ellipsoid zone width as a percentage of baseline allowing comparison with other studies.[21,22]

Results

Cohort Characteristics

We have collected clinical data from 30 patients with biallelic *EYS* variants from 25 families with a median follow-up of 7 years (range, 0–24 years) (Table 1). Twenty-seven patients were diagnosed with RP, two siblings had macular dystrophy, and one isolated patient was diagnosed with CRD. Our multiethnic cohort consisted of 14 patients from European, 13 from Asian, 2 from African, and 1 from mixed European-Asian descent. Nine patients had a history of consanguinity. The current mean age was 45 years (range, 19–75 years), and sex distribution was equal, with 16 patients (53%) being male.

Molecular Diagnosis

Of 27 RP patients, 15 carried compound heterozygous variants (Table 2) and 12 patients had homozygous *EYS* variants, of which 8 reported a history of consanguinity. We found 27 different variants: 8 frame shift, 8 nonsense, 8 indels, 3 missense, and 1 splice site variant (Table 3). Seven of these variants were novel. All missense variants were classified as pathogenic by SIFT and Polyphen2 algorithms and were

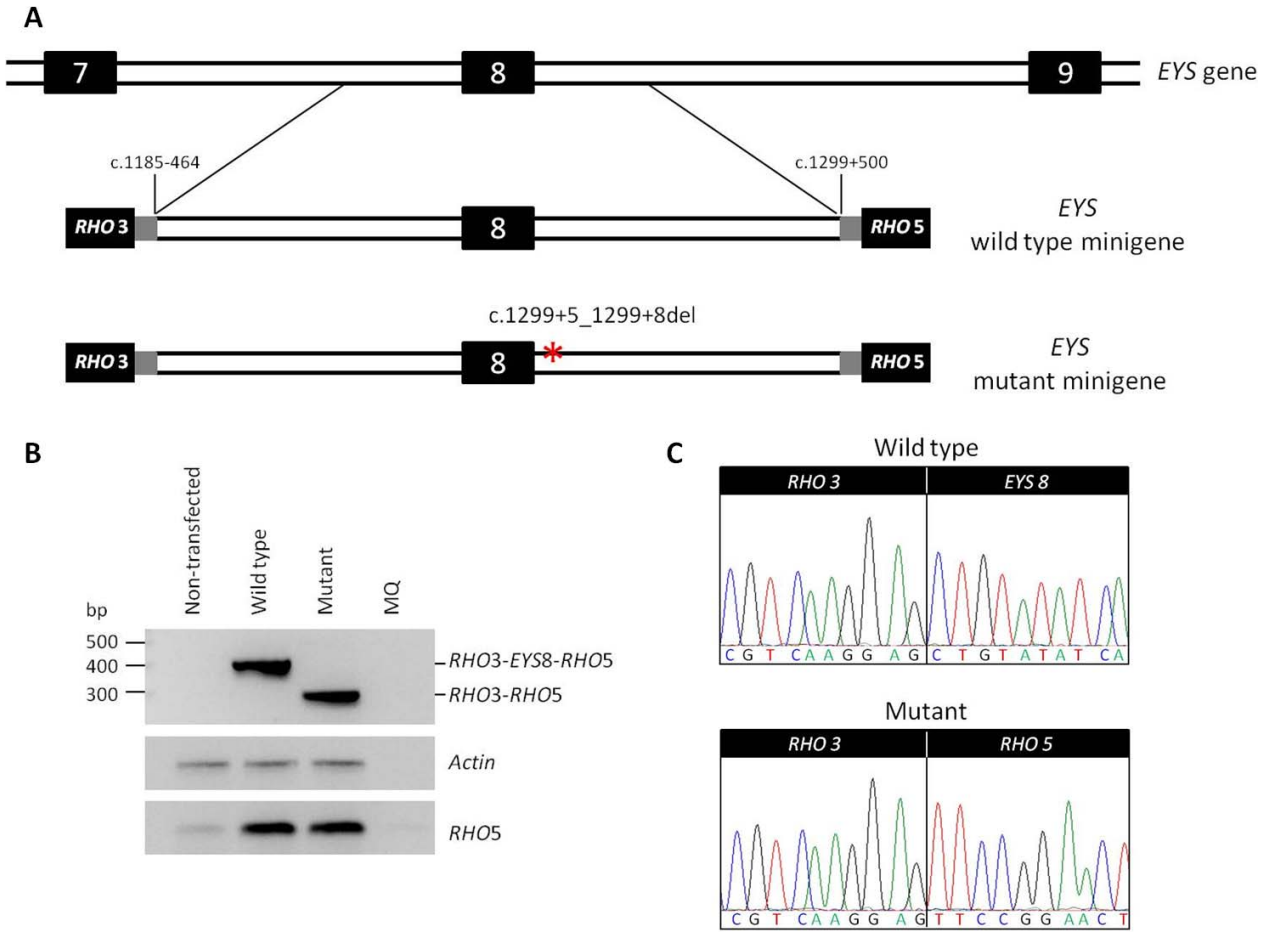

Figure 1. In vitro splice assay showing that the c.1299+5_1299+8del variant results in the skipping of EYS exon 8. (**A**) Schematic overview of the genomic region of *EYS* exon 7 to 9 including the mutation observed in patient XXIV-1 and wild-type and mutant minigenes that were generated. (**B**) RT-PCR analysis of rhodopsin exon 3 (*RHO3*) to rhodopsin exon 5 (*RHO5*), actin (loading control), and rhodopsin exon 5 (transfection control) 48 hours after transfection. The wild-type minigene shows a fragment of ~390 bp, which corresponds to normal splicing (*RHO3-EYS8-RHO5*). The mutant minigene shows a fragment of ~280 bp, which corresponds to *RHO3* and *RHO5* spliced together without *EYS* exon 8. The mutant minigene showed complete exon skipping of *EYS* exon 8. (**C**) Skipping of *EYS* exon 8 (*EYS 8*) in cells transfected with the mutant minigene was validated by Sanger sequencing.

located in conserved residues of EYS protein. According to the American College of Medical Genetics (ACMG) classification, one missense variant, p.(Gly2186Glu), was classified as likely pathogenic and two variants, p.(Arg2604His) and p.(Ile2995Asn), were classified as being of uncertain significance (Table 3).

In patient XXV, diagnosed with CRD, a homozygous *EYS* variant, p.(Tyr3135*) was detected using whole-exome sequencing. Besides this change, no other pathogenic variants were found. The p.(Tyr3135*) variant was previously identified homozygously in two Dutch siblings, namely, one with CRD and one with RP,[4] and three Spanish siblings with RP.[6] In our cohort, two RP patients were heterozygous carriers of this variant.

For patient XXIV-1, diagnosed with macular dystrophy, *ABCA4* was initially screened with Sanger sequencing, but no variants were found. Subsequently, targeted whole-exome sequencing identified two variants in *EYS*, c.1299+5_1299+8del and p.(Gly2017Val).[23] Using Sanger sequencing, we detected these *EYS* variants in his brother, patient XXIV-2. Segregation analysis of the offspring of patient XXIV-1 confirmed that both variants were located on different alleles. The first variant (c.1299+5_1299+8del) was novel, whereas the second variant p.(Gly2017Val) was previously found homozygously in an RP patient.[6] This missense variant was predicted to be pathogenic by in silico prediction tools (Table 3).

Minigene Splice Assay in HEK293T Cells

To investigate potential splice defects associated with the novel c.1299+5_c.1299+8del variant, wild-type and mutant minigenes harboring this change were generated and transfected into HEK293T cells. RT-PCR analysis showed that transfection of the mutant minigene resulted in skipping of *EYS* exon 8, whereas transfection of the wild-type minigene resulted in normal splicing (Fig. 1B). Skipping of *EYS* exon 8 for the mutant minigene was validated by Sanger sequencing (Fig. 1C).

Phenotype and Visual Function of Patients With EYS-Associated RP

Most RP patients developed symptoms of night blindness and VF constriction in the second and third decade of life, and the mean age at diagnosis was 30 years (range, 11–56 years). Demographic information and clinical features are available in

Table 1. Clinical Characteristics of Patients With EYS-Associated Inherited Retinal Dystrophies

Patient ID	Current Age, y, Sex	Age at Diagnosis, y	Age at First Visit, y	Initial Symptoms	Ophthalmic History	Visual Acuity at First Visit, LogMAR		Refractive Error, SE, D		Ophthalmoscopy at Baseline	ffERG Rod Derived	ffERG Cone Derived	ffERG Age	Phenotype
						RE	LE	RE	LE					
I	61, M	56	56	Night blindness, decreased visual acuity (high myopia)	Amblyopia LE, CE BE	0.10	0.52	−7.75	−12.25	Tilted, waxy optic disks with peripapillary atrophy, severe attenuation of the retinal vessels, and bone spicules in the periphery.	NR	NR	56	RP
II-1	43, M	35	35	Night blindness, visual field constriction	Refractive surgery BE for myopia	0.1	0.0	−5.25	−4.25	Waxy optic disks, attenuated retinal vessels, normal aspect of the macula, intraretinal pigmentations in the periphery.	NR	NR	35	RP
II-2	42, F	23	24	Night blindness, decreased visual acuity		0.4	0.3	−4.00	−3.75	Normal aspect of the optic disk, attenuated retinal vessels, preserved posterior pole, and peripheral RPE atrophy and bone spicules.	NR	NR	24	RP
II-3	29, M	16	22	Night blindness		0.1	0.22	−1.50	−0.50	Pallor of the optic disc, attenuated retinal vessels, and peripheral bone spicules and pigment alterations.	NR	NR	22	RP
III	32, M	19	19	Night blindness, decreased visual acuity (CME)	Somatostatin analogue treatment for CME	0.0	0.05	−0.25	−0.50	Pale aspect of the optic disk, attenuated retinal vessels, CME, and peripheral atrophy and bone spicules.	↓↓	↓↓	19	RP
IV	55, F	26	45	Night blindness	CE BE	0.3	0.3	+2.00	NA	Pale aspect of the optic disk, attenuated retinal vessels, Bull's-eye-like maculopathy RE, extensive peripheral atrophy and intraretinal pigmentations.	NP	NP	NA	RP
V	36, M	22	35	Night blindness	CE LE	0.22	0.22	−0.75	−0.50	Waxy optic disks, mild attenuated retinal vessels, peripheral bone spicules.	NP	NP	NA	RP
VI-1	18, F	15	14	Night blindness, visual field constriction		0.22	0.1	−0.50	−0.50	Normal aspect of the optic disks, attenuated retinal vessels, cellophane maculopathy, midperipheral bone spicules and intraretinal pigmentations.	↓↓	↓↓	15	RP
VI-2	21, M	21	21	Night blindness, visual field constriction		0.05	0.15	−0.75	−0.50	Normal aspect of the optic disk, attenuated vessels, absent foveal reflex, and peripheral RPE alterations.	NR	NR	21	RP

Table 1. Continued

Patient ID	Current Age, y, Sex	Age at Diagnosis, y	Age at First Visit, y	Initial Symptoms	Ophthalmic History	Visual Acuity at First Visit, LogMAR		Refractive Error, SE, D		Ophthalmoscopy at Baseline	ffERG Rod Derived	ffERG Cone Derived	ffERG Age	Phenotype
						RE	LE	RE	LE					
VII-1	39, F	35	35	Night blindness, visual field constriction		0.1	0.0	−1.75	−1.25	Waxy optic disks, attenuated retinal vessels, midperipheral bone spicules.	NR	NR	35	RP
VII-2	42, M	40	40	Night blindness, visual field constriction		−0.1	−0.1	−0.50	−2.00	Normal aspect of the optic disks, attenuated retinal vessels, and peripheral bone spicules.	NP	NP	NA	RP
VIII	52, M	40	26	Night blindness		0.05	0.1	−5.25	−4.25	Pale aspect of the optic disk, severely attenuated retinal vessels, pigment alterations in the macular region, RPE atrophy, and bone spicules in the periphery.	NR	NR	40	RP
IX	61, F	46	53	Night blindness	Amblyopia RE, strabismus surgery, CE BE	0.6	0.8	−13.00	−14.00	Pale aspect of the optic disk with peripapillary atrophy, severely attenuated retinal vessels, atrophy of the RPE in the macula, and midperipheral bone spicules.	NR	↓↓	46	RP
X	71, M	38	40	Visual field constriction		0.1	0.1	plano	+1.00	Optic nerve head drusen, severely attenuated retinal vessels, atrophic macular region with foveal island, relatively preserved RPE midperipheral, atrophic RPE in the far periphery with bone spicules, and paving stone degenerations.	NR	↓↓	56	RP
XI	40, F	32	34	Night blindness, decreased visual acuity	CE BE	0.4	0.3	−1.00	−1.00	Pale aspect of the optic disk, attenuated retinal vessels, CME, bone spicules in the midperiphery.	NR	NR	34	RP

Table 1. Continued

Patient ID	Current Age, y, Sex	Age at Diagnosis, y	Age at First Visit, y	Initial Symptoms	Ophthalmic History	Visual Acuity at First Visit, LogMAR		Refractive Error, SE, D		Ophthalmoscopy at Baseline	ffERG Rod Derived	ffERG Cone Derived	ffERG Age	Phenotype
						RE	LE	RE	LE					
XII	34, F	14	26	Night blindness	Refractive laser surgery BE	0.0	0.0	−1.00	−1.25	Pale aspect of the optic disk, severely attenuated retinal vessels, small island with intact RPE in the macula, perimacular creasing of the inner limiting membrane (ILM), extensive lobular atrophy of the RPE in the posterior pole and to periphery, and intraretinal bone spicules on the nasal side.	NR	NR	26	RP
XIII	53, F	53	52	Night blindness, visual field constriction		0.1	0.05	+0.25	+0.5	Normal aspect of the optic disk, mildly attenuated vessels, macula coarsely pigmented, tapetal reflex temporally, RPE atrophy in the far periphery with bone spicule pigmentations.	↓	↓	53	RP
XIV	56, M	50	50	Night blindness, color vision disturbances		0.05	0.0	−7.25	−7.00	Waxy optic disks with peripapillary atrophy, attenuated retinal vessels, perimacular pigment alterations, peripheral bone spicules.	NR	NR	53	RP
XV	66, M		62			0.0	0.4	NA	NA	Pale optic disks, RPE alterations macula, attenuated retinal vessels, midperipheral and peripheral bone spicules.	NR	NR	61	RP
XVI	46, F	26	26	Night blindness, decreased visual acuity	Acetazolamide treatment for CME	0.4	0.1	−5.50	−5.50	Moderate pallor of the optic disk, attenuated vessels, CME, RPE atrophy, and bones spicules in the periphery.	↓↓	↓↓	27	RP
XVII	53, F	11	52	Night blindness, visual field constriction	Cuba therapy BE, CE BE	0.5	0.7	NA	NA	Pale optic disks with peripapillary atrophy, attenuated retinal vessels, normal aspect of the macula, midperipheral, and peripheral bone spicules.	NR	NR	53	RP

Table 1. Continued

Patient ID	Current Age, y, Sex	Age at Diagnosis, y	Age at First Visit, y	Initial Symptoms	Ophthalmic History	Visual Acuity at First Visit, LogMAR		Refractive Error, SE, D		Ophthalmoscopy at Baseline	ffERG Rod Derived	ffERG Cone Derived	ffERG Age	Phenotype
						RE	LE	RE	LE					
XVIII	43, F	21	30	Night blindness		0.05	0.05	NA	NA	Mild pallor optic disk, vessels near normal caliber, preserved RPE in the posterior pole with mild epiretinal membrane formation, RPE changes in the macula with intraretinal crystals. Midperipheral and peripheral atrophy of the RPE RE.	↓↓	↓↓	30	RP
XIX	32, F	27	27	Night blindness	Somatostatin analogue treatment IM for CME	0.0	0.0	+0.50	+0.25	Normal optic disks, attenuated retinal vessels, wrinkling and fibrosis of the ILM, and bone spicules in the far periphery.	NR	↓↓	27	RP
XX	75, M	26	66	Night blindness, visual field constriction	DM II, CE BE	0.6	0.5	NA	NA	Pale excavated optic disks, severely attenuated vessels, and peripheral atrophy of the RPE with bone spicules.	NR	NR	71	RP
XXI	31, F	28	30	Night blindness	Refractive surgery BE for myopia	0.15	0.3	NA	NA	Tilted disks with peripapillary atrophy, attenuated vessels, no bone spicules.	NR	NR	30	RP
XXII	33, M	33	33	Night blindness, visual field constriction		0.2	0.1	−4.00	−3.00	Pink aspect of the optic disks, attenuated vessels, preserved RPE in the posterior pole with mild wrinkling of the ILM LE>RE. Midperipheral mottling of the RPE with intraretinal bone spicule pigmentations.	NP	NP	NA	RP
XXIII	37, F	36	36	Night blindness	CE LE, postoperative steroid-induced glaucoma LE	0.0	0.3	−1.50	−2.00	Moderate pallor of the optic disk, attenuated blood vessels with sheathing, normal aspect of the RPE in the posterior pole, wrinkling of the ILM, and pigment alterations and bone spicule pigmentations in the periphery.	NR	NR	36	RP

Table 1. Continued

Patient ID	Current Age, y, Sex	Age at Diagnosis, y	Age at First Visit, y	Initial Symptoms	Ophthalmic History	Visual Acuity at First Visit, LogMAR		Refractive Error, SE, D		Ophthalmoscopy at Baseline	ffERG Rod Derived	ffERG Cone Derived	ffERG Age	Phenotype
						RE	LE	RE	LE					
XXIV-1	38, M	32	28	Decreased visual acuity, color vision disturbances		0.8	0.8	+0.25	+0.25	Normal aspect of the optic disk, normal retinal vessels, positive foveal reflexes, bull's-eye maculopathy with pigment alterations and tiny white dots.	NL	NL	32	MD
XXIV-2	34, M	18	22	Decreased visual acuity		1.0	0.8	−1.00	−0.50	Normal aspect of the optic disk, normal caliber of the retinal vessels, RPE alterations in the fovea with subfoveal atrophy OD, normal appearance of the peripheral retina.	NL	NL	22	MD
XXV	55, M	55	55	Decreased visual acuity, night blindness	Artisan claw lens implant BE	0.5	0.3	−8.00	−9.00	Pale aspect of the optic disk, attenuated vessels, yellow dots in the macula, peripheral mottling of the RPE.	NR	NR	55	CRD

BE, both eyes; CE, cataract extraction; CME, cystoid macular edema; DM II, diabetes mellitus type 2; F, female; ID, identifier; LE, left eye; M, male; MD, macular dystrophy; IM, intramuscular; NA, not applicable; NL, normal; NP, not performed; NR, no response; RE, right eye; SE, spherical equivalent.

Table 2. Genotype of Patients With EYS-Associated Inherited Retinal Dystrophies (NM_001142800.1)

Patient ID	Nucleotide Change 1	Protein Effect 1	Nucleotide Change 2	Protein Effect 2	Phenotype	Ethnicity
I	c.2308C>T	p.(Gln770*)	c.2308C>T	p.(Gln770*)	RP	Iraq - Asian†
II-1	**c.(331+1_332-1)_(1056+1-1057_1)del**	p.?	**c.(331+1_332-1)_(1056+1-1057_1)del**	p.?	RP	Turkish - Asian†
II-2	**c.(331+1_332-1)_(1056+1-1057_1)del**	p.?	**c.(331+1_332-1)_(1056+1-1057_1)del**	p.?	RP	Turkey - Asian†
II-3	**c.(331+1_332-1)_(1056+1-1057_1)del**	p.?	**c.(331+1_332-1)_(1056+1-1057_1)del**	p.?	RP	Turkey - Asian†
III	c.4350_4356del	p.(Ile1451Profs*3)	c.4350_4356del	p.(Ile1451Profs*3)	RP	Dutch - European†
IV	c.6714del	p.(Ile2239Serfs*17)	c.6714del	p.(Ile2239Serfs*17)	RP	Dutch - European
V	c.4350_4356del	p.(Ile1451Profs*3)	**c.5319_5342del**	p.(Asn1773_Val1781delinsLys)	RP	Dutch - European
VI-1	c.6799_6800del	p.(Gln2267Glufs*15)	c.7095T>G	p.(Tyr2365*)	RP	Dutch - European
VI-2	c.6799_6800del	p.(Gln2267Glufs*15)	c.7095T>G	p.(Tyr2365*)	RP	Dutch - European
VII-1	**c.5928-3_5928-1del**	p.?	**c.5928-3_5928-1del**	p.?	RP	Pakistan – Asian†
VII-2	**c.5928-3_5928-1del**	p.?	**c.5928-3_5928-1del**	p.?	RP	Pakistan - Asian†
VIII	c.5167_5168del	p.(Leu1723Glyfs*6)	**c.(6424-1_6425+1)_(6751+1_6752-1)del**	p.?	RP	Dutch - European
IX	c.4350_4356del	p.(Ile1451Profs*3)	c.7811G>A	p.(Arg2604His)	RP	Dutch - European
X	c.1673G>A	p.(Trp558*)	c.2811C>A	p.(Cys937*)	RP	Dutch - European
XI	c.4955C>G	p.(Ser1652*)	c.8984T>A	p.(Ile2995Asn)	RP	Dutch - European
XII	c.7919G>A	p.(Trp2640*)	c.7919G>A	p.(Trp2640*)	RP	Turkish - Asian
XIII	c.9036del	p.(Leu3013Serfs*6)	c.9405T>A	p.(Tyr3135*)	RP	Dutch - European
XIV	c.4350_4356del	p.(Ile1451Profs*3)	c.6714del	p.(Ile2239Serfs*17)	RP	Dutch - European
XV	c.32dup	p.(Met12Aspfs*14)	c.32dup	p.(Met12Aspfs*14)	RP	Iraq - Asian
XVI	c.1161del	p.(Lys387Asnfs*34)	**c.(2137+1_2137-1)_(2259+1_2260-1)dup**	p.?	RP	Turkish - Asian
XVII	c.4350_4356del	p.(Ile1451Profs*3)	**c.6079-2A>G**	p.?	RP	Dutch - European
XVIII	c.4712C>G	p.(Ser1571*)	c.6557G>A	p.(Gly2186Glu)	RP	South Korea-USA
XIX	c.6714del	p.(Ile2239Serfs*17)	c.1185-3C>T	p.? (splice)	RP	Turkish - Asian
XX	c.1376del	p.(Cys459Serfs*56)	**c.(331+1_332-1)_(862+1_863-1)dup**	p.?	RP	Dutch - European
XXI	c.4045C>T	p.(Arg1349*)	c.4045C>T	p.(Arg1349*)	RP	Turkish - Asian†
XXII	c.8255_8260del	p.(Leu2752_Asn2754delinsTyr)	c.8255_8260del	p.(Leu2752_Asn2754delinsTyr)	RP	Turkish - Asian†
XXIII	c.4350_4356del	p.(Ile1451fs)	c.9405T>A	p.(Tyr3135*)	RP	Dutch – European
XXIV-1	c.1299+5_1299+8del	p.?	c.6050G>T	p.(Gly2017Val)	MD	Morocco – African
XXIV-2	c.1299+5_1299+8del	p.?	c.6050G>T	p.(Gly2017Val)	MD	Morocco – African
XXV	c.9405T>A	p.(Tyr3135*)	c.9405T>A	p.(Tyr3135*)	CRD	Dutch – European

Novel variants are displayed in bold font.
† Consanguinity.

Investigative Ophthalmology & Visual Science

TABLE 3. Missense *EYS* Variants (NM_001142800.1) Identified in This Study and Their In Silico Functional Analyses

Exon	cDNA Change	Protein Change	PhyloP	Grantham	PolyPhen-2 Score	PolyPhen-2 Prediction	SIFT Score	SIFT Prediction	AC (gnomAD)	AF (gnomAD)	Classification
29	c.6050G>T	p.(Gly2017Val)	1.60	109	1.0	Deleterious	0	Deleterious	5	0.00002904	Likely pathogenic
32	c.6557G>A	p.(Gly2186Glu)	2.44	98	0.933	Probably damaging	0	Deleterious	5	0.00003471	Likely pathogenic
40	c.7811G>A	p.(Arg2604His)	1.73	29	0.877	Probably damaging	0	Deleterious	6	0.00003285	Uncertain significance
43	c.8984T>A	p.(Ile2995Asn)	6.32	149	0.996	Deleterious	0	Deleterious	1	0.000006598	Uncertain significance

Classification was assessed according to the ACMG guidelines. AC, allele count; AF, allele frequency.

Table 1. All RP patients had one or more characteristic fundus feature, such as peripheral retinal degeneration, bone spicule pigmentations, attenuated retinal vasculature, or pale waxy optic disc (Supplementary Fig. S2). Refractive error ranged between +2 diopter (D) and −13.5 D, with mean spherical equivalent of −2.75 D. Most patients were mild myopic and three were high myopes (higher than −6 D).

We gathered 146 visual acuity measurements, with a mean of 6 measurements per patient (range, 1–22 measurements). Four patients became visually impaired (BCVA worse than 0.3 logMAR) during follow-up at ages 41, 43, 64, and 70 years and already had constricted VFs (<20°) at earlier examinations. Mixed effects linear regression modeling showed an overall increase in logMAR visual acuity of 0.015 ± 0.002 in the best performing eye per year, which corresponds to a loss of 0.75 Early Treatment Diabetic Retinopathy Study (ETDRS) letters per year ($P < 0.001$) (Fig. 2A).

Fifty-seven Goldmann VF examinations were available, ranging from one to eight measurements per patient. At first examination, 11 patients were visually impaired (central VF radius of the V4e target, <20°) and 5 were blind (central VF radius, <10°). One patient became visually impaired during follow-up at age 39. Ten patients had a central VF larger than 20° at last examination. They did not significantly differ from patients that were visually impaired in terms of age of onset ($P = 0.2262$), age at diagnosis ($P = 0.259$), or age at last examination ($P = 0.136$). All 10 patients carried 2 truncating *EYS* variants, of which 9 were located in the N-terminal part of the protein, and 11 in the C-terminal part. Forty-five VFs from 16 patients, were eligible for longitudinal analysis, and the rate of VF loss of the V4e isopter area was −0.84 ± 0.44 ln(deg^2) per year ($P < 0.001$) (Fig. 2B).

In 23 patients, ffERG was performed: in 15 patients (mean age, 40 years) no scotopic or photopic responses could be elicited, in 5 patients (mean age, 43 years) both scotopic and photopic responses were severely reduced, and in 3 patients (mean age, 29 years) there were no scotopic responses and severely reduced photopic responses.

OCT scans of 24 patients and autofluorescence imaging of 23 patients were available for analysis. In 19 patients, the ellipsoid layer length was shortened but continuous in the foveal area, 16 of them had a hyperautofluorescent ring (Fig. 3B), and 3 had a crescent shape hyperautofluorescence pattern (I, VI-1, and VII-2) (Fig. 3F). In a single patient (VII-1), the ellipsoid layer was continuous over the width of the 4-mm single line scan, accompanied by a crescent shape pattern on autofluorescence imaging. The horizontal ellipsoid zone width in the foveal scan ranged between 0.43 and 5.22 mm (median width, 2.14 mm; $n = 62$) (Fig. 2D). The area of the hyperautofluorescent ring ranged between 0.96 and 13.36 mm^2 (median area, 4.69 mm^2; $n = 24$). The ellipsoid zone width was significantly correlated with the area of the hyperautofluorescent ring, with $r_s = 0.78$ and $P < 0.001$ (Fig. 2C). The rate of decline in ellipsoid zone width was −0.057 ± 0.017 mm per year ($P < 0.01$) ($n = 14$). When calculating the rate of decline as a percentage of baseline, the rate was −3.69% ± 0.51% per year ($P < 0.001$). In patients with a distinguishable hyperautofluorescent ring, the length of the ellipsoid zone was shorter than in patients with a "crescent" autofluorescence pattern, as described by Sengillo et al.[24] (Fig. 3). Four patients (II-2, XV, XVI, and XX) had foveal abnormalities in at least one eye (Fig. 3I, 3J), and it became impossible to discriminate between the different outer retinal layers because retinal architecture in the macula, including the fovea, appeared severely distorted. The majority of RP patients had epiretinal membranes, but there were no patients with macular holes or tractional

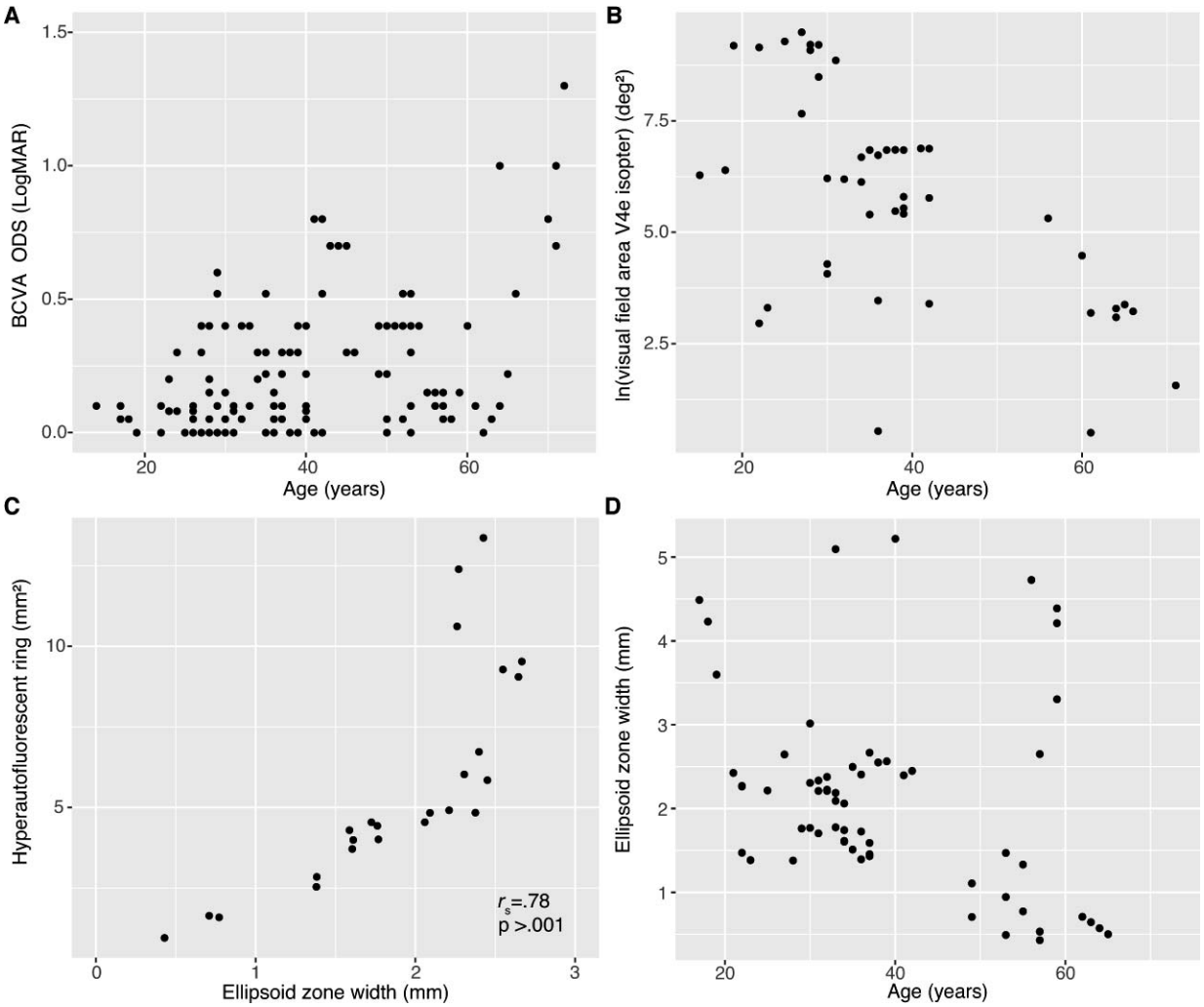

Figure 2. Scatterplots show (**A**) visual acuity versus age, (**B**) visual field area of the V4e isopter versus age, (**D**) ellipsoid zone width versus age, and (**C**) ellipsoid zone width versus hyperautofluorescent ring area.

macular edema. Four patients developed cystoid maculopathy during follow-up, one patient was treated with acetazolamide tablets, and two with somatostatin analogue injections.

Phenotype and Visual Function of a Patient With EYS-Associated CRD

One isolated patient (XXV) noted both a decrease in visual acuity and night blindness as first symptoms, and he previously underwent refractive surgery to correct for high myopia. At first examination, visual acuity was 0.3 logMAR in the best eye. Goldmann VF revealed a central relative scotoma with moderate peripheral constriction (Fig. 4D). On fundoscopy, the optic disks appeared pale, vessels were thin, the macular area displayed thinning of the RPE with a tiny preserved foveal island surrounded by patchy atrophy, and there were subtle RPE changes in the periphery (Fig. 4A). OCT imaging showed atrophy of the outer retinal layers in the posterior pole (Fig. 4B), and fundus autofluorescence showed a hyperautofluorescent ring around the macula and optic nerve, with hypoautofluorescence inside the ring. (Fig. 4C).

Phenotype and Visual Function of Patients with EYS-Associated Macular Dystrophy

The proband (XXIV-2) was the youngest in a family of five siblings; he suffered from decreased visual acuity from the age of 7. He was first examined at age 12, and his binocular visual acuity was 1.0 logMAR with eccentric fixation. At age 22, he was diagnosed with juvenile macular dystrophy, visual acuity was 0.8 logMAR, and funduscopy revealed a bull's eye maculopathy. Central VF testing with Humphrey Field Analyzer 10-2 showed a central scotoma, and color vision testing with Lanthony's desaturated 15-Hue test revealed a tritan defect. ffERG showed normal scotopic and photopic responses. At age 23, pronounced macular atrophy was seen on OCT imaging (Fig. 5G). His older brother (XXIV-1) noted a decrease in visual acuity and color vision problems from the age of 18. At age 32, visual acuity was 0.3 logMAR and funduscopy revealed normal foveal reflexes, perimacular RPE alterations, and few tiny white dots, with normal aspect of the peripheral retina. OCT imaging showed atrophy of the ellipsoid zone in the fovea, and fundus autofluorescence revealed a hyperautofluorescent ring (Figs. 5A–C). At age 36, ffERG rod and cone responses were within normal range, and multifocal electroretinogram showed

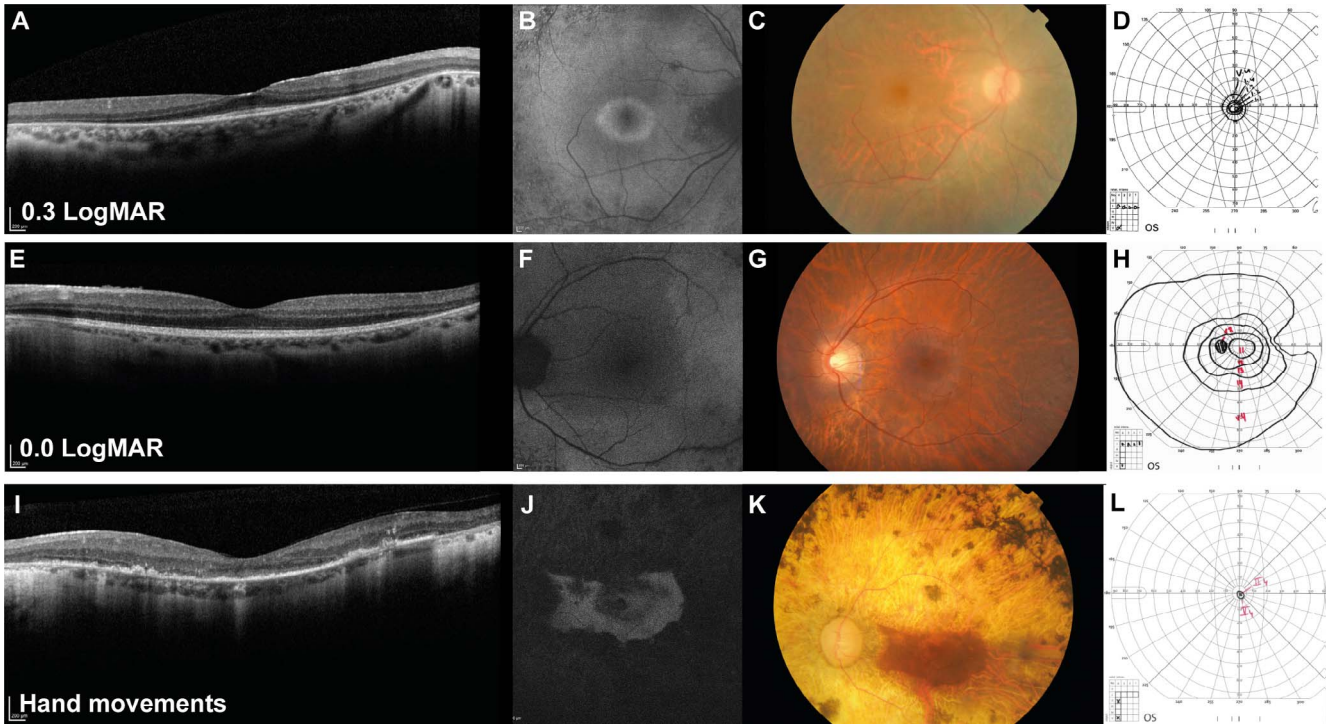

Figure 3. Optical coherence tomography, fundus autofluorescence, fundus photography, and visual field of three RP patients with different RP phenotypes. Patients II-3 (age 23) shows a typical RP phenotype with (**A**) shortening of the ellipsoid layer length and (**B**) a hyperautofluorescent ring surrounding the fovea, (**C**) the optic disk appears pale and vessels are narrow. Visual field (**D**) is severely constricted (~10°). Patient VII-2 (age 41) has a milder phenotype, (**E**) the ellipsoid layer length is longer, and there is (**F**) a "crescent-shaped" hyperautofluorescent pattern visible. (**G**) The optic disk appears pink and vessels are narrow. There is decreased sensitivity of the peripheral visual field (**H**), with an absolute scotoma nasally. Patient XX (age 73) has end-stage RP, and (**I**) the ellipsoid zone and other outer segment layers are no longer discernible. There is a (**J**) small relatively hyperautofluorescent patch in the perifoveal area, surrounded by hypoautofluorescence, and the fovea itself appears hypoautofluorescent as well. In fundo (**K**), the optic disk appears pale, vessels are very narrow, and there is extensive atrophy of the RPE and choriocapillaris with bone spicule pigmentations. A small island of RPE remains in the macula with RPE-alterations. The visual field (**L**) is severely constricted (<10°).

decreased foveal responses (Supplementary Fig. S3). At age 38, visual acuity was 0.7 logMAR and OCT imaging showed atrophy of all outer retinal layers and thinning of the RPE. Fundus autofluorescence revealed a larger hyperautofluorescent ring surrounding the hypoautofluorescent macula (Figs. 5D and 5F).

Discussion

In this study, we have assessed the spectrum of retinal disease and the course of visual function in 30 patients carrying biallelic *EYS* variants. Twenty-seven patients had RP, one patient had CRD, and two patients had macular dystrophy, based on clinical characteristics, functional testing, and retinal imaging. *EYS* mutations are one of the most common causes of autosomal recessive retinitis pigmentosa in Asia and Europe. Novel findings included the presence of homozygous *EYS* mutations in CRD patients and compound heterozygous *EYS* mutations in patients with macular dystrophy.

The age of onset in RP patients ranged from 7 to 51 years, and all had one or more typical fundus features corresponding with RP (Supplementary Fig. S1). Four patients became visually impaired (BCVA worse than 0.3 logMAR) during follow-up at ages 41, 43, 64, and 70 years. Mixed effects linear regression

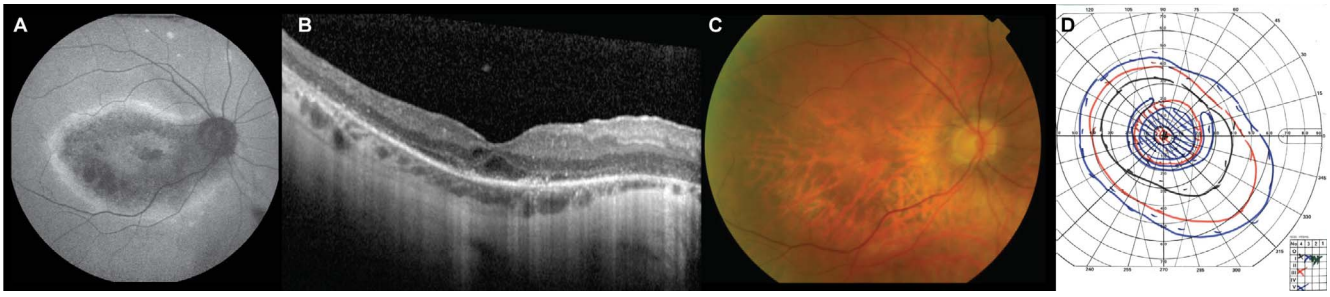

Figure 4. Autofluorescence, SD-OCT, and fundus pictures of patient with CRD. (**A**) Fundus autofluorescence of patient XXV shows a hyperautofluorescent ring within the vascular arcade, surrounding the macular area, which appears patchy, with diffuse hypoautofluorescent lesions. The fovea appears hypoautofluorescent. (**B**) On OCT, there is a foveal empty space, the outer retinal layers are distorted, and the ellipsoid zone can no longer be distinguished. (**C**) Atrophy of the posterior pole with discernable choroidal vasculature, and the retinal vessels are attenuated. (**D**) Goldmann visual field reveals a relative central scotoma with mild to moderate peripheral constriction.

Investigative Ophthalmology & Visual Science

Figure 5. Infrared imaging, OCT imaging, and fundus photography in patients with macular dystrophy. Disease progression of EYS-associated macular dystrophy in patient XXIV-1 by using SD-OCT scans, FAF, and fundus images of the right eye. (**A–C**) At age 32, SD-OCT scan shows foveal atrophy with local disruption of the ellipsoid zone and thinning of the outer nuclear layer, and on FAF a hyperautofluorescent ring is discernable surrounding the fovea. Fundus photograph reveals a normal optic disk, normal caliber of the retinal vessels, and subtle RPE alterations in the foveal region but no abnormalities in the peripheral retina. (**D–F**) At age 38, SD-OCT shows progression of the foveal atrophy with disruption of the inner retinal layers, hyperreflective deposits, and thinning of the RPE. FAF shows a more advanced bull's-eye maculopathy with a hypo-autoflorescent fovea and a hyperreflective ring. Fundus photograph reveals a hypopigmented fovea surrounded by RPE alterations and RPE atrophy, and there were no peripheral abnormalities. (**G**) SD-OCT of patient XXIV-2 at age 23, showing macular atrophy.

modeling showed an overall increase in logMAR visual acuity of 0.015 in the best performing eye per year, which corresponds to a loss of 0.75 ETDRS letters per year ($P < 0.001$). One study in a heterogeneous group of RP patients found a decline in visual acuity of 2.3 ETDRS letters per year. This would place *EYS*-associated RP in the milder spectrum of disease.[25] Based on VF constriction, 11 out of 27 RP patients were visually impaired (41%) and 5 were blind (19%) according to World Health Organization criteria at first examination in our centers. The rate of peripheral VF loss for the V4e target was -0.84 ± 0.44 ln(deg^2) per year in our cohort. McGuigan et al.[21] reported the rate as −23% of normal per year. Ten RP patients had a central VF larger than 20° at last follow-up (mean age, 39 years). They did not differ from RP patients with VF constriction in age of onset or age at last examination. All 10 of these patients carried compound heterozygous or homozygous truncating variants.

Differences in disease manifestation and progression are often attributed to a difference in underlying causal variants (e.g. missense versus truncating variants). Three out of 27 RP patients carried 1 heterozygous missense *EYS* variant, and 1 truncating *EYS* variant. There were no patients with homozygous missense *EYS* variants; therefore, we could not study whether missense variants were associated with milder retinal disease in our cohort. Siblings with the same *EYS* genotype can differ substantially in age of onset, disease presentation, and rate of disease progression. Our study was not suited to determine genotype-phenotype correlations in detail, as many variants were observed only once.

The estimated decline in ellipsoid zone width was -57 ± 17 µm per year, which was less than in previous publications where yearly decline varied between −76.4 µm to −248 µm.[25–29] However, these estimates were based on RP patients with different underlying genetic defects and inheritance modes. We also calculated the rate of shortening as a

percentage from baseline to enable comparison with two studies in EYS patients. Our estimate was −3.69% ± 0.51%, which corresponds with the findings of two previous studies, reporting a rate of −4.65% ± 2.89% ($n = 12$)[22] and −5.6% ± 2.6% per year ($n = 4$).[21]

Two-thirds of RP patients in our cohort had typical hyperautofluorescent rings, and one-third had a crescent shape hyperautofluorescent pattern, as described by Sengillo et al.[24] The crescent pattern was associated with larger VFs and, therefore, milder disease progression. Three out of four patients had two mutations near the C-terminal domain, which could have a less detrimental impact on protein structure or function. Additional studies would be most helpful to study the effect of these mutations on the different isoforms.

Three cases of *EYS*-associated CRD have been published so far; the first case was a Dutch patient that carried the same homozygous variant as our CRD patient, p.(Tyr3135*).[4] The second case was a Japanese patient, carrying compound heterozygous *EYS* variants, p.(Tyr2935*) and p.(Ser1653fs). Segregation analysis confirmed that these variants were located on different alleles. Each separate variant homozygous, as well as the identical compound heterozygous combination of these variants, were previously identified as causal in RP patients.[9,30–32] The third case was a French patient with compound heterozygous variants, p.(Trp558*) and p.(Asn745Ser). The pathogenicity of the missense variant was questionable, as it proved to be not conserved, and the pathogenicity is uncertain according to the ACMG classification.[18] The homozygous nonsense variant p.(Tyr3135*) that our CRD patient as well as the first mentioned CRD case carried was also detected in RP patients,[4,5] including in two RP patients of this cohort. The variant is located in the last *EYS* exon and leads to a premature stop codon. Functional assays might reveal whether the variant leads to nonsense-mediated decay or the formation of a C-terminal-truncated EYS protein. It is unclear why identical genotypes can result in both RP and CRD phenotypes. The *EYS* variants found in CRD patients did not cluster in a specific domain. Of the four known *EYS* isoforms, only the two long isoforms (isoform 1 and 4) are predicted to be affected by the mutations, as all CRD-associated variants are all located after the 594th amino acid. Unfortunately, this does not help explain the difference in phenotype because some of the underlying genotypes were also found in RP patients. The presence of genetic and epigenetic modifiers, or environmental factors, could also play a role in the observed differences in phenotype in these patients.

Macular dystrophy is an IRD in which the central retina is primarily affected and peripheral photoreceptor function is spared. Patients XXIV-1 and XXIV-2 presented with an isolated macular dystrophy, with a normal ffERG. Targeted whole-exome sequencing identified compound heterozygous *EYS* variants: c.1299+5_1299+8del and c.6050G>T. To assure the functional effect of the splice site variant, we generated a mutant minigene. RT-PCR analysis showed that transfection of the mutant minigene resulted in skipping of *EYS* exon 8, suggesting that similar missplicing events can occur in the retina. This variant has not been described in other IRD patients; therefore, it is not clear whether this variant is solely associated with macular dystrophy or can also lead to other phenotypes. Exon 8 codes for the fifth EGF-like domain that is part of all four known EYS isoforms. EGF-like domains are usually located in the extracellular domain of membrane-bound proteins, such as EYS, and are important for the structural integrity of the protein. The second variant, c.6050G>T, was previously found homozygous in an RP patient.[6] *EYS* is expressed in the outer segments of both rods and cones and is thought to be crucial for the stability of the ciliary axonema and photoreceptor homeostasis in humans. In several mammal lineages, such as rodents, *EYS* is not expressed, which limits the availability of animal models that better mimic human anatomy and physiology. *EYS* zebrafish knockout studies showed CRD pattern of retinal degeneration,[16] and RP or macular dystrophy phenotypes have not been described in animals that are mutant for *Eys*.

Because molecular testing can uncover pathogenic variants in genes that have not been associated with the phenotype of interest, it remains crucial to perform segregation analysis and to keep looking for variants in other genes. Reassessing the phenotype might be worthwhile, especially in patients with end-stage disease in whom discriminating between different subtypes of IRD might prove difficult, as both central and peripheral retinal architecture are frequently severely distorted. To better understand the pathophysiology of *EYS*-associated IRDs, it is essential to perform functional studies that focus on the effect of mutations on the different *EYS* isoforms and their effect within the retina.

Acknowledgments

Supported by the Foundation Combined Ophthalmic Research Rotterdam (CORR), Rotterdam, The Netherlands (LHMP).

Disclosure: **L.H.M. Pierrache**, None; **M. Messchaert**, None; **A.A.H.J. Thiadens**, None; **L. Haer-Wigman**, None; **Y. de Jong-Hesse**, None; **W.A.G. van Zelst-Stams**, None; **R.W.J. Collin**, None; **C.C.W. Klaver**, None; **L.I. van den Born**, None

References

1. Hartong DT, Berson EL, Dryja TP. Retinitis pigmentosa. *Lancet*. 2006;368:1795–1809.
2. Verbakel SK, van Huet RAC, Boon CJF, et al. Non-syndromic retinitis pigmentosa. *Prog Retin Eye Res*. 2018;66:157–186.
3. Abd El-Aziz MM, Barragan I, O'Driscoll CA, et al. EYS, encoding an ortholog of Drosophila spacemaker, is mutated in autosomal recessive retinitis pigmentosa. *Nat Genet*. 2008; 40:1285–1287.
4. Collin RW, Littink KW, Klevering BJ, et al. Identification of a 2 Mb human ortholog of Drosophila eyes shut/spacemaker that is mutated in patients with retinitis pigmentosa. *Am J Hum Genet*. 2008;83:594–603.
5. Littink KW, van den Born LI, Koenekoop RK, et al. Mutations in the EYS gene account for approximately 5% of autosomal recessive retinitis pigmentosa and cause a fairly homogeneous phenotype. *Ophthalmology*. 2010;117:2026–2033.
6. Barragan I, Borrego S, Pieras JI, et al. Mutation spectrum of EYS in Spanish patients with autosomal recessive retinitis pigmentosa. *Hum Mutat*. 2010;31:E1772–E1800.
7. Arai Y, Maeda A, Hirami Y, et al. Retinitis pigmentosa with EYS mutations is the most prevalent inherited retinal dystrophy in Japanese populations. *J Ophthalmol*. 2015;2015:819760.
8. Bandah-Rozenfeld D, Littink KW, Ben-Yosef T, et al. Novel null mutations in the EYS gene are a frequent cause of autosomal recessive retinitis pigmentosa in the Israeli population. *Invest Ophthalmol Vis Sci*. 2010;51:4387–4394.
9. Iwanami M, Oshikawa M, Nishida T, et al. High prevalence of mutations in the EYS gene in Japanese patients with autosomal recessive retinitis pigmentosa. *Invest Ophthalmol Vis Sci*. 2012;53:1033–1040.
10. Abd El-Aziz MM, O'Driscoll CA, Kaye RS, et al. Identification of novel mutations in the ortholog of Drosophila eyes shut gene (EYS) causing autosomal recessive retinitis pigmentosa. *Invest Ophthalmol Vis Sci*. 2010;51:4266–4272.
11. Audo I, Sahel JA, Mohand-Said S, et al. EYS is a major gene for rod-cone dystrophies in France. *Hum Mutat*. 2010;31:E1406–E1435.

12. Katagiri S, Akahori M, Hayashi T, et al. Autosomal recessive cone-rod dystrophy associated with compound heterozygous mutations in the EYS gene. *Doc Ophthalmol*. 2014;128:211–217.
13. Boulanger-Scemama E, El Shamieh S, Demontant V, et al. Next-generation sequencing applied to a large French cone and cone-rod dystrophy cohort: mutation spectrum and new genotype-phenotype correlation. *Orphanet J Rare Dis*. 2015; 10:85.
14. Alfano G, Kruczek PM, Shah AZ, et al. EYS is a protein associated with the ciliary axoneme in rods and cones. *PLoS One*. 2016;11:e0166397.
15. Zelhof AC, Hardy RW, Becker A, Zuker CS. Transforming the architecture of compound eyes. *Nature*. 2006;443:696–699.
16. Lu Z, Hu X, Liu F, et al. Ablation of EYS in zebrafish causes mislocalisation of outer segment proteins, F-actin disruption and cone-rod dystrophy. *Sci Rep*. 2017;7:46098.
17. Yu M, Liu Y, Li J, et al. Eyes shut homolog is required for maintaining the ciliary pocket and survival of photoreceptors in zebrafish. *Biol Open*. 2016;5:1662–1673.
18. Messchaert M, Dona M, Broekman S, et al. Eyes shut homolog is important for the maintenance of photoreceptor morphology and visual function in zebrafish. *PLoS One*. 2018;13: e0200789.
19. Dagnelie G. Conversion of planimetric visual field data into solid angles and retinal areas. *Clin Vision Sci*. 1990;5:95–100.
20. Iannaccone A, Kritchevsky SB, Ciccarelli ML, et al. Kinetics of visual field loss in Usher syndrome type II. *Invest Ophthalmol Vis Sci*. 2004;45:784–792.
21. McGuigan DB, Heon E, Cideciyan AV, et al. EYS mutations causing autosomal recessive retinitis pigmentosa: changes of retinal structure and function with disease progression. *Genes (Basel)*. 2017;8:178.
22. Miyata M, Ogino K, Gotoh N, et al. Inner segment ellipsoid band length is a prognostic factor in retinitis pigmentosa associated with EYS mutations: 5-year observation of retinal structure. *Eye (Lond)*. 2016;30:1588–1592.
23. Haer-Wigman L, van Zelst-Stams WA, Pfundt R, et al. Diagnostic exome sequencing in 266 Dutch patients with visual impairment. *Eur J Hum Genet*. 2017;25:591–599.
24. Sengillo JD, Lee W, Nagasaki T, et al. A distinct phenotype of eyes shut homolog (EYS)-retinitis pigmentosa is associated with variants near the C-terminus. *Am J Ophthalmol*. 2018; 190:99–112.
25. Iftikhar M, Usmani B, Sanyal A, et al. Progression of retinitis pigmentosa on multimodal imaging: The PREP-1 study. *Clin Exp Ophthalmol*. Available at: https://www.ncbi.nlm.nih.gov/pubmed/30552737. Accessed April 30, 2019.
26. Takahashi VKL, Takiuti JT, Jauregui R, et al. Structural disease progression in PDE6-associated autosomal recessive retinitis pigmentosa. *Ophthalmic Genet*. 2018;39:610–614.
27. Sujirakul T, Lin MK, Duong J, et al. Multimodal imaging of central retinal disease progression in a 2-year mean follow-up of retinitis pigmentosa. *Am J Ophthalmol*. 2015;160:786–798.e4.
28. Cabral T, Sengillo JD, Duong JK, et al. Retrospective analysis of structural disease progression in retinitis pigmentosa utilizing multimodal imaging. *Sci Rep*. 2017;7:10347.
29. Birch DG, Locke KG, Wen Y, et al. Spectral-domain optical coherence tomography measures of outer segment layer progression in patients with X-linked retinitis pigmentosa. *JAMA Ophthalmol*. 2013;131:1143–1150.
30. Oishi M, Oishi A, Gotoh N, et al. Comprehensive molecular diagnosis of a large cohort of Japanese retinitis pigmentosa and Usher syndrome patients by next-generation sequencing. *Invest Ophthalmol Vis Sci*. 2014;55:7369–7375.
31. Suto K, Hosono K, Takahashi M, et al. Clinical phenotype in ten unrelated Japanese patients with mutations in the EYS gene. *Ophthalmic Genet*. 2014;35:25–34.
32. Hosono K, Ishigami C, Takahashi M, et al. Two novel mutations in the EYS gene are possible major causes of autosomal recessive retinitis pigmentosa in the Japanese population. *PLoS One*. 2012;7:e31036.

Investigative Ophthalmology & Visual Science